Fundamental Methods to Measure the Orbital Angular Momentum of Light

Berkhout, G.C.G.

CHAPTER 5

Quantitative mapping of the optical vortices in a speckle pattern

In previous chapters, we have demonstrated that a multi-pinhole interferometer can be used to measure the topological charge of an optical vortex. We further showed that this method can be used to find the optical vortices in a speckle pattern. Here, we show that a multi-pinhole interferometer can also be used to make a two-dimensional map of an optical field in terms of radially independent optical vortex components, $\exp(im\phi)$, where m is an integer. From these maps, we can not only determine the position and topological charge of the optical vortices in the field, but also their anisotropy and their orientation. We present results for an isotropic optical vortex and a speckle pattern containing several vortices. The results from the latter case can serve as the starting point to experimentally study the statistics of the anisotropy and orientation of optical vortices in a speckle pattern.

G. C. G. Berkhout, Y. O. van Boheemen, M. P. van Exter, and M. W. Beijersbergen, in preparation for publication.

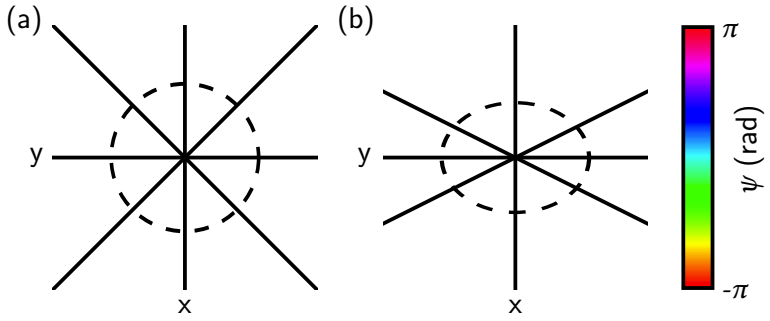

Figure 5.1: Phase of the field for (a) an isotropic $\ell = 1$ optical vortex and (b) an anisotropic $\ell = 1$ optical vortex. The black lines indicate equal phase lines and are spaced $\pi/4$ radians apart. In (b) the lines are more closely spaced around the y axis, showing the anisotropic character of the vortex. In addition, the dashed lines indicate lines of constant intensity. For an isotropic optical vortex, the lines of constant intensity are circles, while for an anisotropic optical vortex they are ellipses.

5.1 Introduction

Optical vortices are of great importance in optics, both for their fundamental properties and their connection to the orbital angular momentum of light [1, 25], as well as for their applications in optical communication [30, 33] and coronography [21].

Optical vortices are associated with phase singularities in an optical field. Isotropic or pure optical vortices are characterised by a complex amplitude whose azimuthal behaviour is characterised by, $A(\phi) \propto \exp(i\ell\phi)$, where ℓ is the topological charge, i.e., the integer number of multiples of 2π that the phase of the field increases in a full turn around the vortex. For an isotropic optical vortex, this phase increase goes linear with the azimuthal coordinate, ϕ. However, in general, this phase increase does not have to be linear, in which case the vortex is called anisotropic (see figure 5.1 for a comparison). Not only does the phase increase in a nonlinear fashion around an anisotropic vortex, also the intensity profile around it is anisotropic, meaning that the lines of constant intensity are ellipses [44], which is indicated by the dashed lines in figure 5.1. Describing the azimuthal behaviour of the field around an anisotropic optical vortex requires more than one pure optical vortex mode, such that the field can be decomposed in the orthogonal basis of pure vortex modes

$$A(\phi) = \sum_{m} \frac{\lambda_m}{\sqrt{2\pi}} e^{im\phi}, \tag{5.1}$$

where the factor $1/\sqrt{2\pi}$ ensures normalization. The coefficient λ_0 is related to the local intensity of the field, while the coefficients λ_{-1} and λ_1 are related to the derivatives of the field. In the case of an isotropic optical vortex, $\lambda_m = \delta_{m,\ell}$, where $\delta_{i,j}$ is the Kronecker delta.

Anisotropic optical vortices occur in speckle patterns, which arise naturally from the

interference of a large number of more or less random plane waves. At particular places in a speckle pattern the amplitude of the field vanishes, causing the phase to be singular. Around these phase singularities an optical vortex is formed, whose exact form is determined by the local interference of the plane waves. Several parametrisations have been proposed to characterise the behaviour of the field around such a vortex. In [9], Freund introduced two parameters to describe the field, which he called the anisotropy and skewness. However, the division between anisotropy and skewness depends on the overall phase of the optical field. This was pointed out by Schechner and Shamir [45], who claimed that the parameters introduced by Freund are inconvenient as "they are not functionally independent of each other." The true independent parameters are the anisotropy of the vortex and the orientation of the major semi-axis of the ellipse shown in figure 5.1 (b). A detailed description of these parameters is given in [32, 44, 46]. In [44], the statistical distributions of the anisotropy and orientation in a speckle pattern are given. Experimental verification of the distribution of the anisotropy has been shown in [38].

A convenient way to find the optical vortices is to interfere the speckle pattern with a reference beam [8, 38, 47], which allows reconstruction of the phase around the phase singularity. From this phase reconstruction, the topological charge, anisotropy and orientation of the optical vortex can be determined.

In previous chapters we have described a different method to measure the topological charge of an optical vortex using a multi-pinhole interferometer (MPI). In chapter 4, we have shown that this method also works for finding optical vortices in a speckle pattern. Here, we demonstrate that we can use an MPI to map a field in terms of its pure optical vortex components, in other words, that we can find the coefficients λ_m for each position in the field. From these coefficients, we can determine the position of the optical vortices and their topological charges as well as their anisotropy and orientation.

We present results for an isotropic optical vortex with $\ell = -1$ and a speckle pattern. The latter case can serve as a starting point for studying the statistics of the anisotropy and orientation of the optical vortices in a speckle pattern.

5.2 Theory

A general MPI consists of N pinholes with diameter b, positioned equidistantly on the circumference of a circle with radius a. Provided that the pinholes do not overlap, the transmission function of the MPI, $T(x, y)$, is given by

$$T(x, y) = \sum_{k=0}^{N-1} \mathrm{circ}(x - x_k, y - y_k), \tag{5.2}$$

where

$$\mathrm{circ}(x,y) = \begin{cases} 1 & \text{if } \sqrt{x^2+y^2} \le b/2 \\ 0 & \text{if } \sqrt{x^2+y^2} > b/2 \end{cases}, \tag{5.3}$$

and $(x_k, y_k) = (a\cos\alpha_k, a\sin\alpha_k)$ is the centre of the k-th pinhole with $\alpha_k = 2\pi k/N$. The diffraction pattern behind the MPI is given by

$$I(u,v) \propto \left|\mathcal{F}\{A(x,y)T(x,y)\}\right|^2, \tag{5.4}$$

where $A(x,y)$ is the complex field incident on the MPI, and $\mathcal{F}$ denotes the Fourier transform. If the pinholes are small compared to the scale of the fluctuations in the incident field, the amplitude and phase of this field can be considered to be constant over the area of a pinhole, and the diffraction pattern can be written as (see [27, 41])

$$I(u,v) \propto \left|\sum_{k=0}^{N-1} A_k \mathcal{F}\{\mathrm{circ}(x-x_k, y-y_k)\}\right|^2, \tag{5.5}$$

where $A_k = |A_k|\exp(i\phi_k)$ is the complex amplitude of the field incident on the k-th pinhole and $|A_k|$ and ϕ_k are the amplitude and phase respectively. If the MPI is illuminated with an optical vortex, the observed diffraction patterns depend in a qualitative way on the topological charge of the vortex [27]. A more quantitative analysis of the diffraction patterns is presented in [41]; this analysis is based on taking the numerical Fourier transform of the diffraction patterns, which is given by

$$g(x,y) \propto \mathcal{F}^{-1}\{I(u,v)\} \tag{5.6}$$

$$\propto \sum_{k,l=1}^{N-1} P_{kl} A_k A_l^*, \tag{5.7}$$

where * denotes the complex conjugate and

$$P_{kl}(x,y) = \int \mathrm{circ}(\alpha - x_k, \beta - y_k)\mathrm{circ}(\alpha - x_l - x, \beta - y_l - y)\,d\alpha\,d\beta, \tag{5.8}$$

and the integral is taken over the entire area of the image. Although the input of the Fourier transform is a real-valued intensity image, $I(u,v)$, its output $g(x,y)$ is complex valued. Moreover, $g(x,y)$ is the convolution of the complex field just after the MPI with its complex conjugate. In the special case that the MPI consists of an odd number of pinholes and the diameter of the pinholes is not more than half the separation between them, $g(x,y)$ consists of a number of discrete peaks that are located at $(x_k - x_l, y_k - y_l)$ and given by

$$g(x_k - x_l, y_k - y_l) \propto A_k A_l^*, \tag{5.9}$$

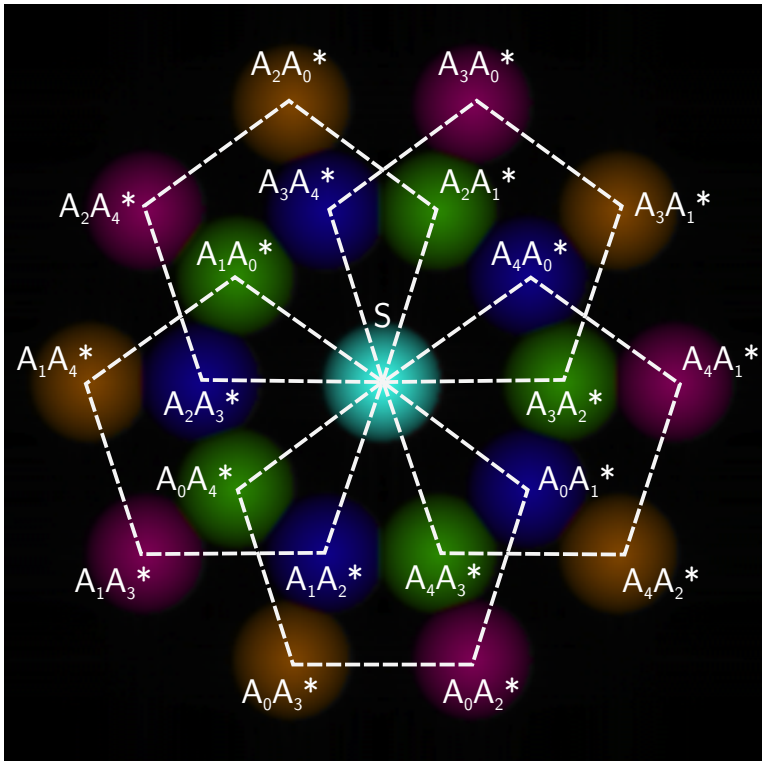

Figure 5.2: Graphical representation of equation 5.9 for an $N = 5$ multi-pinhole interferometer illuminated with an on-axis and centred $\ell = 1$ optical vortex. Each of the 20 spots corresponds to a cross-product, $A_k A_l^*$. In addition, the central peak is given by $S = \sum_{k=0}^{N-1} |A_k|^2$. As a guide to the eye, $N = 5$ dashed pentagons are drawn, which will be used in the analysis described in section 5.3.

where A_k and A_l are the complex amplitudes at the k-th and l-th pinhole, respectively. Interestingly, each peak corresponds to a single product of the amplitudes at two pinholes. Figure 5.2 shows a typical example of equation 5.6 for $N = 5$. Because the input signal of the Fourier transform, $I(u, v)$, is real valued, $g^*(x, y) = g(-x, -y)$ which can be clearly seen in the figure.

From the set of cross-products, $A_k A_l^*$, the amplitude of the field at each of the pinholes can be determined (details of this analysis are provided in section 5.3). Once the complex amplitudes are determined, these can be rewritten in the basis of radially independent optical vortex modes

$$A_k = \sum_{m=-(N-1)/2}^{(N-1)/2} \frac{\lambda_m}{\sqrt{2\pi}} e^{im(2\pi k/N)}. \tag{5.10}$$

As explained in chapter 2, an MPI with and odd number of pinholes N can only detect N

different vortex modes and hence the summation in equation 5.10 runs from $m = -\frac{N-1}{2}$ to $m = \frac{N-1}{2}$. We further define $\gamma_m \equiv |\lambda_m|^2$.

Once we have decomposed the field in the aforementioned basis, we can use the results to calculate the anisotropy and orientation of the optical vortex using the equations given in [44]

$$s_3 = \frac{\gamma_1 - \gamma_{-1}}{\gamma_1 + \gamma_{-1}}. \tag{5.11}$$

Finally, we can calculate the orientation of the optical vortex by

$$\phi_o = \frac{1}{2}(\arg \lambda_1 - \arg \lambda_{-1}). \tag{5.12}$$

5.3 Analysis

To extract the complex amplitudes at the pinholes from the diffraction patterns behind an MPI, we apply the following analysis steps:

1. Centre the diffraction patterns on the CCD-image and crop the image;
2. Calculate the inverse discrete Fourier transform (IDFT);
3. Determine the complex peak amplitudes of all $N(N-1)+1$ peaks in the IDFT image;
4. Derive the complex amplitudes, A_k, at the pinholes;
5. Rewrite these amplitudes in terms of the radially independent vortex modes (coefficients λ_k);
6. Calculate the anisotropy and orientation of the optical vortex.

Below we describe these steps in more detail.

Due to the fact that the MPI moves, while the CCD-camera is fixed, the diffraction pattern moves across the CCD-camera as the stage moves, which affects the Fourier transform of the image. To avoid this, we first determine the centre of the diffraction patterns by making use of the Bessel function amplitude envelope, caused by the diffraction at the individual pinholes. We do so by convoluting the diffraction pattern with the Bessel pattern expected from a single pinhole and determining the maximal overlap between the two images, which corresponds to the centre of the diffraction pattern. Once the centre of the diffraction pattern is determined, the pattern is shifted such that its centre coincides with the centre of the image, by circularly rotating the pixels in both the x and y direction. The original image has 768×512 pixels. After centring, the image is cropped to 512×512 pixels, by removing 128 columns of pixels on either side of the image.

We take the complex discrete Fourier transform of this centred and cropped image, which returns an image as described by equation 5.9. Due to the fact that we use a discrete

Fourier transform, the position, (x_{kl}, y_{kl}), and diameter, s, of all $N(N-1)+1$ peaks in the Fourier transformed image is scaled and given by

$$(x_{kl}, y_{kl}) = \frac{n_{\sim} d}{\lambda z_{\sim}}(x_k - x_l, y_k - y_l), \tag{5.13}$$

$$s = \frac{n_{\sim} d}{\lambda z_{\sim}} b, \tag{5.14}$$

where a and b are the dimensions of the multi-pinhole interferometer, $z_{\sim} = 0.1$ m is the distance between the MPI and the CCD, $\lambda = 633$ nm is the wavelength, $n_{\sim} = 512$ is the number of pixels, and $d = 9.0$ µm is the pixel size. For convenience, we define $S_{kl} \equiv A_k A_l^*$ and use the positions given in equation 5.13 as a starting point for finding the peak amplitudes $|S_{kl}|$. The absolute value of the complex amplitude around these peaks, $|g(x,y)|$ around these peaks is described by the convolution between two pinholes which is described by

$$|g(x,y)| = c\sqrt{(x - x_{kl})^2 + (y - y_{kl})^2} + |S_{kl}|, \tag{5.15}$$

where c is a negative constant. We fit this function to the amplitude of the transformed image around each of the peak positions (x_{kl}, y_{kl}) and find the peak amplitudes $|S_{kl}|$. The phase can be directly determined from the phase of $g(x,y)$, which can be combined with $|S_{kl}|$ to give the complex value of S_{kl}. In addition, we determine the peak amplitude of the central peak in the Fourier transform, S. To do this, we perform a fitting routine similar to the one described in equation 5.15, but remove the central pixel of the Fourier transform, since this pixel alone contains all the background offset of the original image.

From this set of S_{kl}, we can determine the complex amplitude of the field at the pinholes. For each fixed value of l, we can apply the following analysis. For demonstration purposes, we take $l = 0$ and use

$$A_k A_0^* \equiv S_{k0}, \tag{5.16}$$

for $k = 1 \ldots N-1$. In addition, the intensity of the central peak of the Fourier transformation is given by

$$\begin{aligned} S &= \sum_{k=0}^{N-1} |A_k|^2 \\ &= |A_0|^2 + \sum_{k=1}^{N-1} \left|\frac{S_{k0}}{A_0}\right|^2, \end{aligned} \tag{5.17}$$

where we used equation 5.16 to get to the second part of this equation. Equation 5.17 can be solved for A_0

$$|A_0| = \sqrt{\frac{1}{2}\left(S - \sqrt{S^2 - 4S_0}\right)}, \tag{5.18}$$

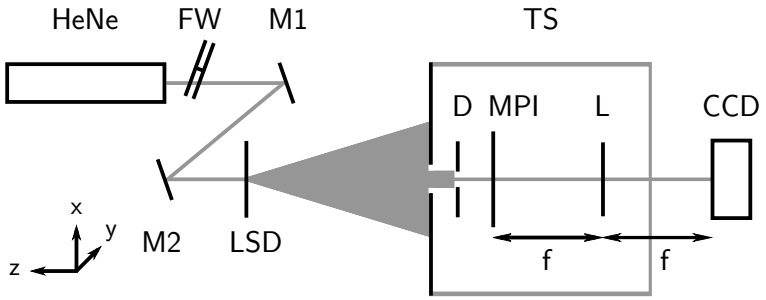

Figure 5.3: Schematic overview of the setup used to measure a map of the pure vortex modes in a complex field, and thereby the position, charge, anisotropy and orientation of the vortices contained in the field. We use the setup to study the far-field of a fully developed speckle pattern, which is generated by illuminating a light shaping diffuser (LSD) with a helium-neon (HeNe) laser beam. The LSD can be replaced by a fork hologram, which produces isotropic optical vortices. Two mirrors (M1 and M2) and a filter wheel (FW) are used to steer and attenuate the beam. The MPI is mounted on a translation stage (TS) that can moved in the x- and y-direction. An iris (D) is used to shield the MPI from any stray light. The far-field diffraction pattern behind the MPI is recorded with a lens (L) and a CCD-camera, which is fixed to the optical table.

where $S_0 = \sum_{k=1}^{N-1} |S_{k0}|^2$. Since we can determine the field up to an overall phase, we choose the phase of A_0 to be 0. From equation 5.16 and the obtained values for S_{k0} we can now determine A_k for $k = 1 \ldots N-1$. This analysis can be repeated for $l = 1 \ldots N-1$, which reduces the noise in the determined amplitudes.

Finally we rewrite the obtained complex amplitudes in the basis of radially independent optical vortex modes using equation 5.10 and calculate the anisotropy and orientation of the vortex using equations 5.11 and 5.12, respectively.

5.4 Experiment

To experimentally measure a map of the pure vortex modes in a complex field, and thereby the position, charge, anisotropy and orientation of the vortices contained in the field, we use the setup shown in figure 5.3. In this particular experiment we use an MPI with $N = 5$, $a = 100$ µm and $b = 50$ µm. The stage is used to scan the MPI through the far-field of a fully developed speckle pattern that is generated by illuminating a light shaping diffuser with a helium-neon laser (see figure 5.3 and its caption for more details). The diffuser can be replaced by a fork hologram which generates isotropic optical vortices. For each position of the translation stage the diffraction pattern is captured using the CCD-camera; the image is analysed directly as described above, to avoid storage of large amounts of data.

5.5 Results

To demonstrate the validity of our method, we first analyse the far-field of a fork hologram, which contains an isotropic optical vortex in each of its diffraction orders, except for the zeroth order. We choose the diffraction order that contains a vortex with $\ell = -1$. This vortex is studied with the setup presented previously, where we scanned the MPI in 20 by 20 steps of 20 µm. The results of the analysis are shown in figure 5.4, were we show $\gamma_{m_\mathcal{L}} \equiv |\lambda_{m_\mathcal{L}}|^2$, for $m_\mathcal{L} = 0, \pm 1, \pm 2$. As expected, only the γ_{-1} shows a contribution in the centre of the beam. At the beams edges, the beam starts resembling a flat wave front and, indeed, the γ_0 components becomes dominant.

From the above results, we can derive the anisotropy and orientation of the optical vortices. For the case of the isotropic $\ell = -1$ vortex, we obtain

$$s_3 = 1.00, \tag{5.19}$$

$$\phi_0 = -0.441\pi, \tag{5.20}$$

which proves that our system gives the expected result.

Subsequently, we study a speckle pattern which is scanned with 200 by 200 steps of 20 µm (see figure 5.5). Following the same method, we can calculate the anisotropy and orientation of the vortices in the speckle patterns. The γ_0 components is proportional to the locally averaged intensity of the field and it indeed resembles the intensity of a speckle pattern. One can see several optical vortices of both charge $\ell = -1$ and $\ell = 1$, which show up as bright spots in the γ_{-1} and γ_1 images, respectively. The results from this analysis serve as a starting point for a statistical analysis of the anisotropy and orientation of optical vortices in a speckle pattern.

5.6 Conclusion

We have demonstrated that an MPI can be used to map a field in terms of its optical vortex components. These maps can not only be used to find the positions and topological charges of the optical vortices in the field, but also to determine their anisotropy and orientation. We have presented results for a field with an isotropic optical vortex, which proves the validity of the analysis. In addition, we have shown the optical vortex maps for a speckle pattern, which contains several optical vortices. By studying a large number of these optical vortices, one can determine the statistics and the anisotropy and orientation of these vortices; this is subject for further study.

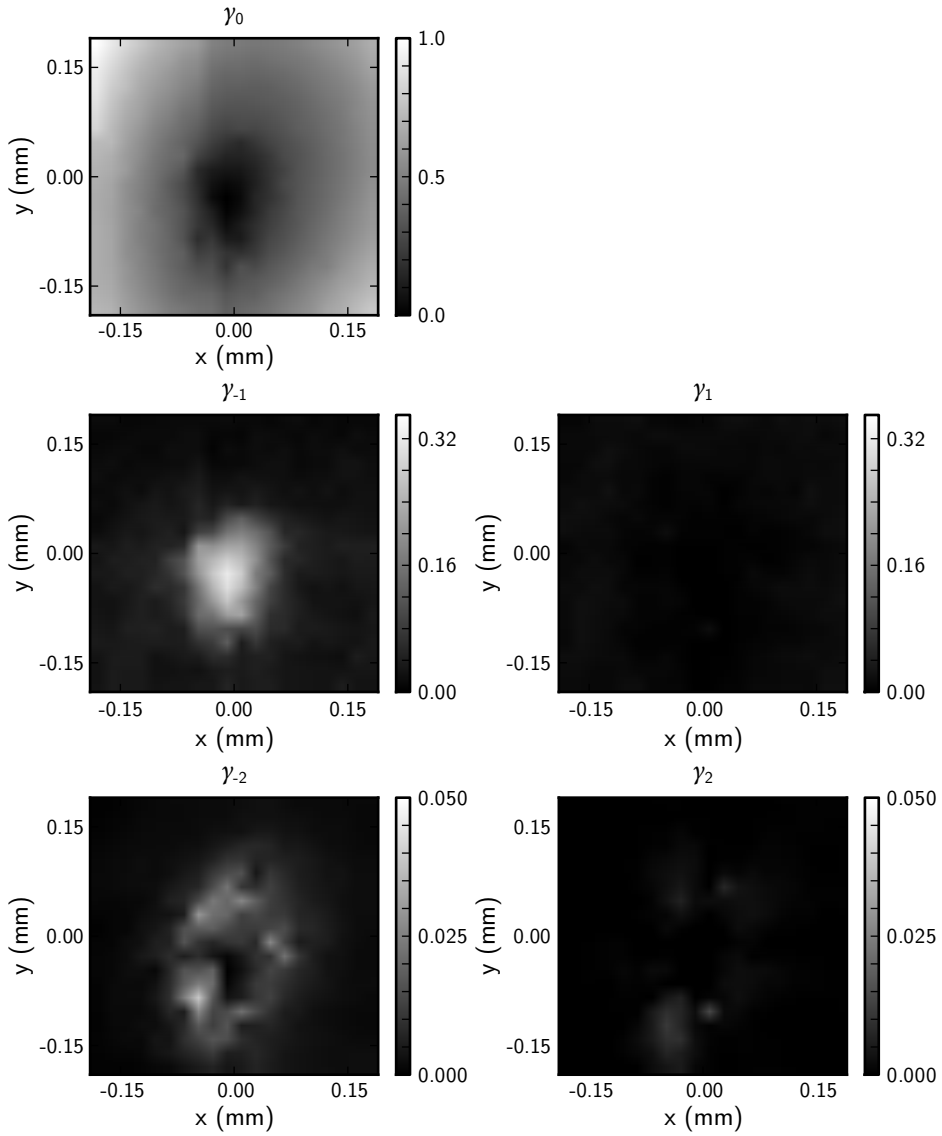

Figure 5.4: Coefficients of the radially independent optical vortex modes in an isotropic $\ell = -1$ optical vortex. As expected only the γ_{-1} is present in and around the centre of the beam. Further away from the centre of the beam, the wave front becomes flatter and γ_0 gives the highest contribution. All images are normalised to the peak of the γ_0 image.

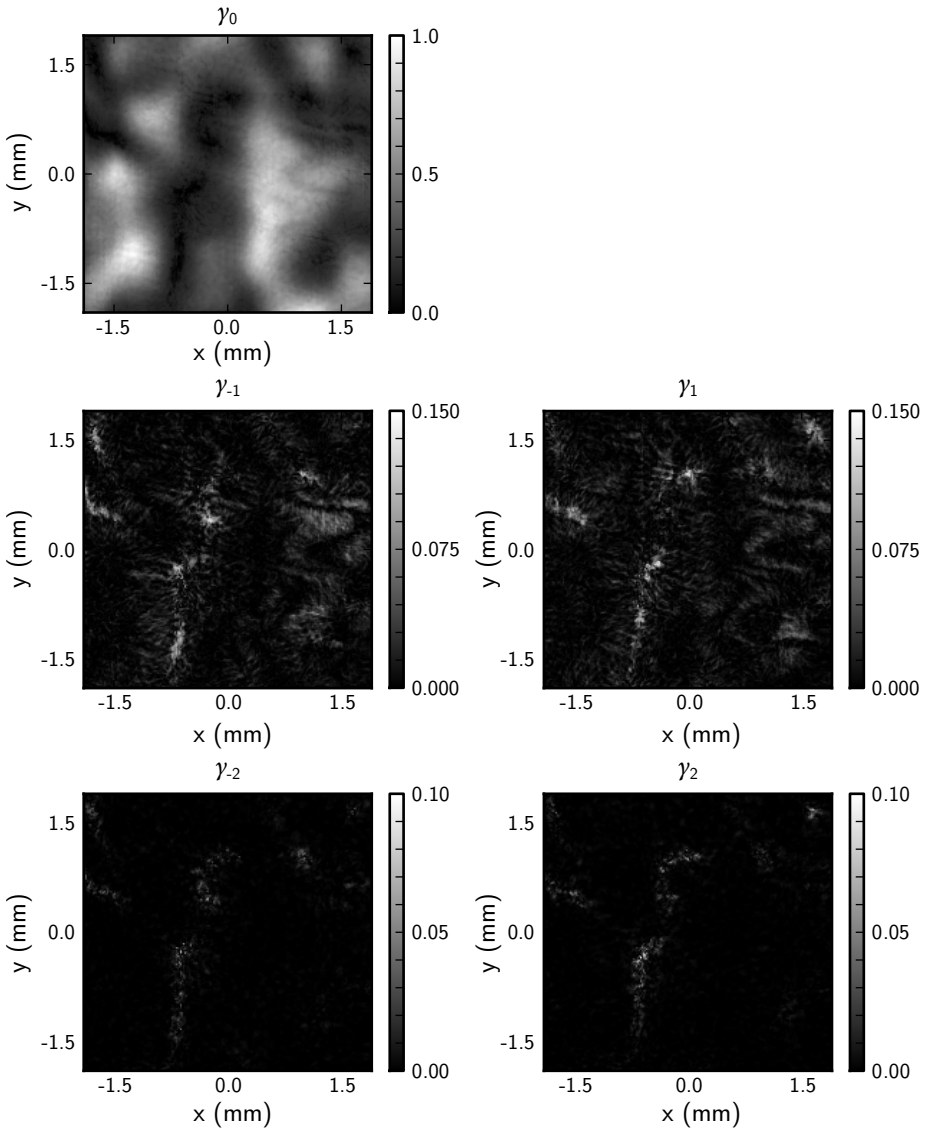

Figure 5.5: Coefficients of the radially independent optical vortex modes in a speckle patterns. The γ_0 is proportional to the locally averaged intensity and indeed resembles an image of a speckle pattern. Several optical vortices, both of topological charge $\ell = -1$ and $\ell = 1$, can be seen as bright spots in the γ_{-1} and γ_1 images, respectively. Detailed study of the area around each vortex will yield the anisotropy and orientation of each of the vortices.